CANCER

Multiepitope tissue analysis reveals SPPL3-mediated ADAM10 activation as a key step in the transformation of melanocytes

2017 © The Authors, some rights reserved; exclusive licensee American Association for the Advancement of Science

Christian Ostalecki, ^{1*} Jung-Hyun Lee, ^{1*} Jochen Dindorf, ¹ Lena Collenburg, ¹ Stephan Schierer, ¹ Beate Simon, ¹ Stefan Schliep, ¹ Elisabeth Kremmer, ² Gerold Schuler, ¹ Andreas S. Baur^{1†}

The evolution of cancer is characterized by the appearance of specific mutations, but these mutations are translated into proteins that must cooperate to induce malignant transformation. Using a systemic approach with the multiepitope ligand cartography (MELC) technology, we analyzed protein expression profiles (PEPs) in nevi and BRAF^{V600E}-positive superficial spreading melanomas (SSMs) from patient tissues to identify key transformation events. The PEPs in nevi and SSMs differed predominantly in the abundance of specific antigens, but the PEPs of nevi- and melanoma-associated keratinocytes gradually changed during the transformation process. A stepwise change in PEP with similar properties occurred in keratinocytes cocultured with melanoma cells. Analysis of the individual steps indicated that activation of the metalloproteinase ADAM10 by signal peptide peptidase–like 3 (SPPL3) triggered by mutant BRAF^{V600E} was a critical transformation event. SPPL3-mediated ADAM10 activation involved the translocation of SPPL3 and ADAM10 into Rab4- or Rab27-positive endosomal compartments. This endosomal translocation, and hence ADAM10 activation, was inhibited by the presence of the tumor suppressor PTEN. Our findings suggest that systematic tissue antigen analysis could complement whole-genome approaches to provide more insight into cancer development.

INTRODUCTION

Enormous progress has been made in identifying so-called driver mutations causing the malignant transformation of melanocytes (1, 2). Overall, the results suggested a "many roads lead to Rome" scenario, consisting of highways with typical mutations in few key molecules and less frequented roads with rare genetic changes. In addition, DNA amplifications are frequently observed, indicating that protein concentrations have a role in the transformation process (3, 4). However, on the protein level, the early transformation events are less understood.

Because melanomas harbor a high number of different genomic mutations, protein expression profiles (PEPs) could differ significantly within and in-between early melanomas and in comparison to nevi. On the other hand, the growth pattern of superficial spreading melanomas (SSMs) is rather similar and typically follows, at first, a radial/apical and then a vertical growth direction. Moreover, in nevi, the sequel of mutation events is frequently unidirectional and cumulative; the ${\rm BRAF}^{{\rm V}600{\rm E}}$ mutation is often present years before additional mutations give rise to a cancer cell (5, 6). The concept of a common transformation path, at least in histologically defined subsets of melanomas, is supported by the occurrence of many primary and secondary oncogenic events in the same genes, like from the RAS-RAF-MEK [mitogen-activated protein kinase (MAPK) kinase]-MAPK and the phosphatidylinositol 3-kinase (PI3K)-AKT pathways (7, 8). One mutation in either pathway (BRAF $^{\mathrm{V}600\mathrm{E}}$ or PTEN inactivation) induces metastatic melanoma in a mouse model (9). In line with a functional convergence on the protein level, we previously reported that 30 of 31 primary melanoma cell lines harbor activated ADAM10 (a disintegrin and metalloproteinase domain-containing protein 10) (10).

Melanocytes communicate with keratinocytes through gap junctions formed by a large family of proteins termed connexins (11, 12). A

homeostatic intercellular exchange of factors as well as connexins themselves are believed to suppress neoplastic transformation (12–14), which seems necessary as healthy skin cells accumulate numerous mutations (15). The cell-to-cell delivery of molecules may change because, for example, keratinocytes express different connexins upon malignant melanocyte transformation (16). Furthermore, transformed melanocytes modulate their cell-to-cell connections, apparently communicating more among themselves and with fibroblasts (17). However, although it is assumed that these morphological and molecular alterations are required for the transformation process, the precise role of the keratinocyte environment for the malignant transformation process is incompletely understood.

The robot-automated multiepitope ligand cartography (MELC) technology (18) permits the side-by-side staining of tissue sections with up to 100 antibodies and more, allowing one to assess topographical PEPs in tissue sections. We used this technology to search for key events in the malignant transformation of melanocytes, systematically comparing PEPs of different nevi and different stages of SSM. Whereas the PEP of both cell types differed mainly in abundance, the PEP in surrounding keratinocytes showed markedly distinct and conserved alterations in the profile constituents that reflected the transformation process. Our analysis provided unexpected insights, revealing that mutations, protein abundance, and subcellular localization of crucial factors, as well as possibly the early microenvironment, cooperate in a stepwise self-stimulating manner before malignant transformation occurs and autonomous proliferation ensues.

RESULTS

Nevi and melanoma PEPs differ in the abundance of selected antigens

To obtain antibodies applicable in the MELC technology, 814 randomly selected hybridoma supernatants from the antibody production facility of the Helmholtz Center in Munich and 173 commercially available antibodies were subjected to a screening algorithm (fig. S1) to obtain those antibodies giving a specific staining in the tissue (epidermis and

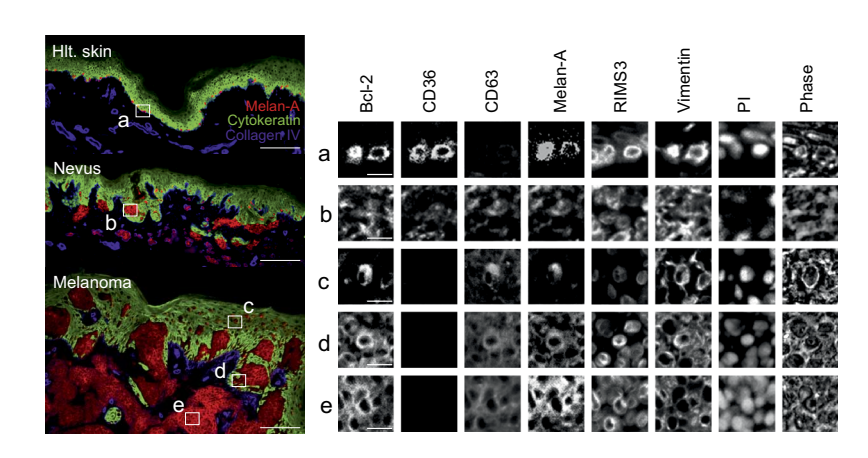
¹Department of Dermatology, University Hospital Erlangen, Translational Research Center, Schwabachanlage 12, 91054 Erlangen, Germany. ²Institute of Molecular Immunology, Helmholtz-Zentrum München, Marchioninistraße 25, D-81377 Munich, Germany. *These authors contributed equally to this work.

[†]Corresponding author. Email: andreas.baur@uk-erlangen.de

dermis) for melanoma cells (n = 57; table S1). We reasoned that key factors of the transformation process would appear in melanomas but not in nevi. We also selected antibodies that were specific for melanoma-associated keratinocytes (n = 7) or for melanomas and keratinocytes (n = 12) (table S1). Single tissue sections of six BRAF^{V600E+} SSM (fig. S2), six junctional (three) and compound (three) nevi, and six samples of healthy skin were stained by the whole antibody set. For each antigen, we determined the average relative abundance using an equation integrating gray value intensities of the background and 6 to 30 different staining areas for each sample (fig. S3). Almost all antibodies gave a positive staining with melanocytes, nevi, and melanoma tissue. There were only few exceptions; CD63 was detected only in nevi and melanoma, and CD36 was only found in melanocytes and nevi (Fig. 1A). However, the relative abundance of selected antigens differed significantly. Nevi showed a more than twofold increase in 6 of 57 antigens over melanocytes, and melanoma cells further increased abundance of 10 of 57 antigens, including those increased in nevi, such as CD63, CD71, and phosphorylated extracellular signal-regulated kinase 1 (ERK1) and ERK2 (ERK1/2) (Fig. 1B, red bars in middle and bottom panels). A number of proteins were also reduced in concentration of greater than twofold in nevi compared to melanocytes (12 of 57; blue bars) and in melanoma cells compared to nevi (6 of 57; blue bars). Thus, protein abundance of key proteins changed rather uniformly across different samples and potentially had a role in the transformation process.

To substantiate this assumption, we compared PEPs in three different layers of the SSMs, namely, in the basal layer, apical layer, and dermal layer, because dermal layer cells have a more aggressive growth behavior (19). Dermal layer cells showed the highest protein abundance in all layers (Fig. 1B, top panel). In comparison to the basal layer, increases of more than twofold were seen in 5 of 57 antigens (arrows). When we compared cells in the apical and dermal layers, the abundance of

many factors (16 of 57) relative to that in the basal layer diverged in an opposing manner, meaning some were increased in the cells of one layer but decreased in the other (Fig. 1B, boxes). Among those was the histone deacetylase Sirtuin-2 (red box), the function of which hints at one possible explanation (transcriptional regulation) for the divergent PEPs between the apical and dermal layers. Together, higher abundance of 10 to 20% of antigens seemed to correlate with malignant transformation



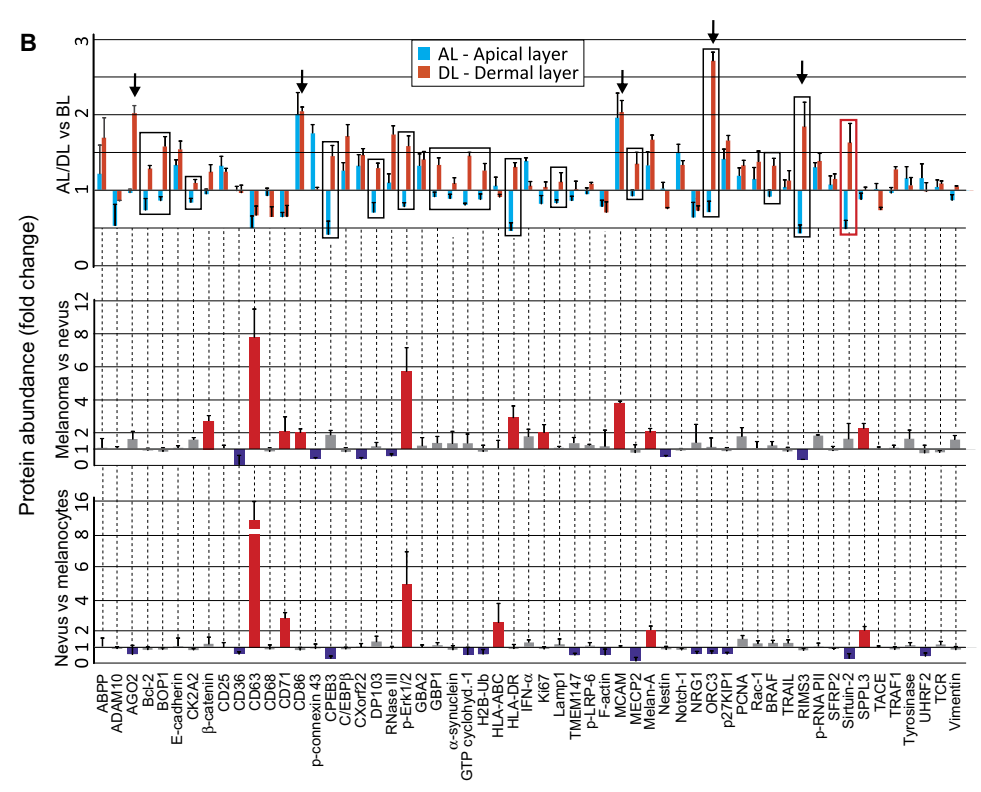


Fig. 1. Nevi and melanoma PEPs differ. (**A**) Left: Representative staining for Melan-A, cytokeratin, and collagen IV in melanocytes [healthy (Hlt.) skin], a compound nevus, and an SSM. Right: Representative analysis by MELC for six markers and propidium iodide (PI) in the corresponding tissue areas marked by boxes a to e in the left histology images. All panels across each horizontal row at the right were from the same tissue section denoted on the left by lowercase letters. Scale bars, $100 \, \mu m$ (left) and $10 \, \mu m$ (right). (**B**) Fold increase or decrease in the abundance of 57 markers (see also fig. S2) in compound nevi relative to healthy melanocytes (lower graph), in melanoma cells relative to compound nevi (middle graph), and in melanoma apical layer (AL) and dermal layer (DL) cells relative to basal layer (BL) cells (upper graph). Data are means \pm SEM from six samples, quantified as gray value intensity relative to the background in 6 to 30 different regions of interest for each sample analyzed (see example in fig. S3).

and a more aggressive growth behavior of melanoma cells. However, these results did not indicate crucial events of the transformation process.

Melanoma cells modulate the PEP of associated keratinocytes

We noticed that the PEP of keratinocytes adjacent to SSM, but not to benign nevi, changed visibly (fig. S4A) and followed an all-or-nothing expression phenotype for numerous factors (Fig. 2A). To confirm this finding, we cultured different primary melanoma cells (ML01, ML03, ML05, ML07, and ML11) that had been characterized previously (10) with keratinocytes (HaCaT cells) and noticed that all melanoma cells formed dendritic connections (Fig. 2B). We placed melanoma cells on one side of a keratinocyte colony and analyzed their PEP by MELC after 72 hours. In a gradient-type fashion, the PEP and subcellular localization of selected factors changed in the keratinocytes (Fig. 2C, arrow in upper left image). These changes were very similar to those seen between nevi and SSM in tissue sections (Fig. 2C). A systematic analysis of melanoma cell- and SSM-associated keratinocytes (n = 6 each condition) confirmed their overall similar PEP (Fig. 2D; summary in table S2). Thus, the transfer of certain effectors to keratinocytes was a conserved function of melanoma cells.

The keratinocyte PEP mirrors the melanocyte transformation process

In view of these results, we speculated that melanocyte transformation occurred in discernable steps, potentially mirrored by the keratinocyte PEP. Thus, we systematically compared keratinocyte PEPs in healthy skin, junctional nevi, compound nevi, halo nevi, and dysplastic nevi, as well as in BRAF^{V600E+} SSMs with horizontal, vertical, and invasive growth patterns (fig. S5). A progressive change in the keratinocyte PEP was observed from those associated with healthy skin to those associated with melanoma (Fig. 3 and fig. S6A). Patterns in the changing PEPs included factors that seemingly disappeared, gradually appeared and increased in abundance, extended their expression into additional keratinocyte layers, or changed their subcellular localization. Whereas changes started at the level

of benign nevi with low abundance of interferon- α (IFN- α), CD63, and signal peptide peptidase–like 3 (SPPL3), major differences were seen between the dysplastic nevi and the early SSM. This included the seemingly complete loss of p27^{KIP1}, ADAM10, and its substrate Notch1 (Fig. 3, images outlined in red).

We previously demonstrated ADAM10 activation in 30 of 31 primary melanoma cell lines (10) and therefore hypothesized that the loss of ADAM10 and Notch1 staining was the result of a loss or masking of the antibody epitope upon maturation and cleavage of the protease and its substrate (20). An enhancement of the fluorescence signal in melanoma-associated keratinocytes revealed a weak nuclear staining for Notch1 (fig. S4B) and residual presence of ADAM10 (Fig. 4A, bottom panel). To confirm ADAM10 processing, we generated an antibody against the C terminus of the protease and were then able to visualize ADAM10 in

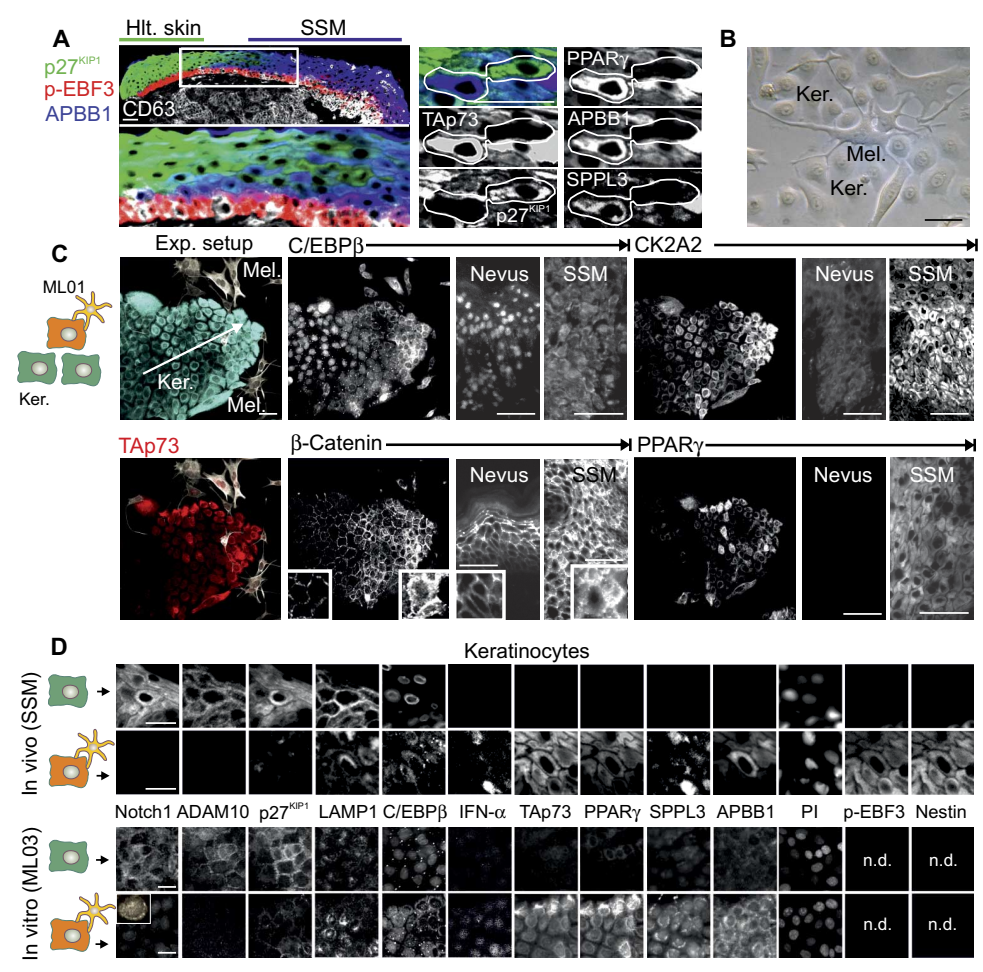


Fig. 2. Keratinocytes in association with melanoma cells change their PEP. (**A**) A tissue section representing the transition from healthy epidermis (Hlt. skin; p27^{KIP1}, green) to melanoma (SSM; CD63, white) was stained for the indicated markers (right), which show an all-or-nothing staining phenotype (summary in table S2). Scale bar, 50 μm. (**B**) Coculture of melanoma cells (Mel.) with keratinocytes (Ker.), showing melanoma cells in contact with keratinocytes. Scale bar, 50 μm. (**C**) Coculture of ML01 melanoma cells with keratinocytes and PEP analysis of selected markers by MELC. For comparison, representative keratinocyte tissue sections from nevi and SSM were stained for the indicated markers. Scale bars, 50 μm. The arrow indicates the expression gradient. Graphics, left: Cube cells, keratinocytes (orange denotes contact with melanoma cells); astral cells, melanoma. (**D**) Systematic comparison of the indicated PEPs of healthy keratinocytes (rows marked by green graphic) and melanoma-associated keratinocytes (orange + astral graphic) in tissue sections (healthy skin and SSM) (top) and ML03/HaCaT cocultures (bottom), obtained by MELC analysis. Scale bars, 25 μm. Lower left image: The inset shows a representative cell with increased fluorescence to demonstrate nuclear Notch1 staining. n = 6 for each condition. n.d., not detected.

melanoma-associated keratinocytes (Fig. 4A). To confirm ADAM10 activation, we used an indicator protein, consisting of pro-tumor necrosis factor (proTNF) fused to green fluorescent protein (GFP) at the N terminus and red fluorescent protein (RFP) at the C terminus (G-proTNF-R) (Fig. 4B). G-proTNF-R appears yellow under ultraviolet light but emits a green (GFP-pro) and red (TNF-RFP) moiety upon its cleavage by activated ADAM10 or ADAM17 (10). In keratinocytes not connected to melanoma cells, no cleavage of G-proTNF-R occurred, whereas melanoma-associated keratinocytes harbored predominantly cleaved TNF-RFP (Fig. 4B). This effect was observed in different melanoma cells and was quantified as described previously (10) by counting the number of yellow and red vesicular compartments (Fig. 4B, graph). Because our previous report (10) showed that only ADAM10 and not ADAM17 was activated in primary melanoma lines, these data

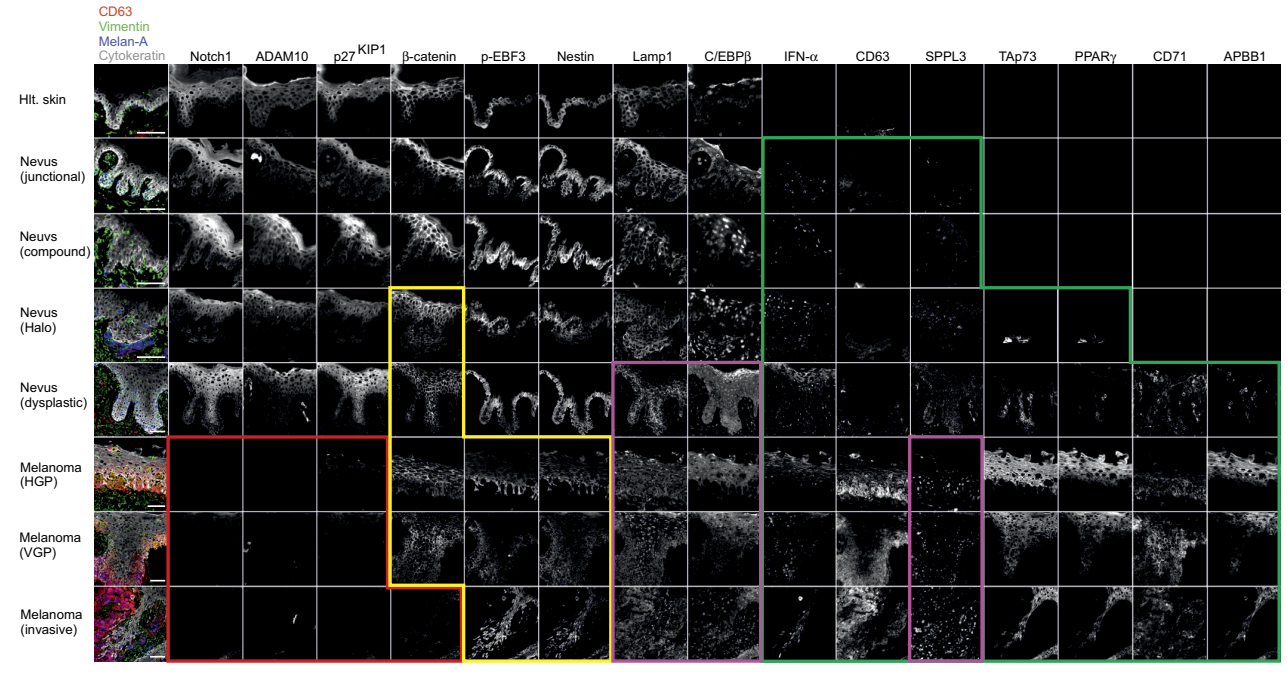


Fig. 3. The keratinocyte PEP reflects the transformation process from nevi to melanoma. Keratinocyte tissue areas from healthy skin, various nevi, and melanomas (left colored panels and fig. S5) (n = 6 for each condition) were systematically analyzed by MELC for keratinocyte-specific markers as listed in table S2. The most prominent and representative results are presented in fig. S6. Red outlined images, proteins exhibiting lost abundance in progressive stages; green, proteins exhibiting increased abundance in progressive stages; yellow, proteins exhibiting an extended expression into additional keratinocyte/epidermal layers; magenta, proteins that exhibited a change in subcellular localization in progressive stages. Scale bars, 50 μ m.

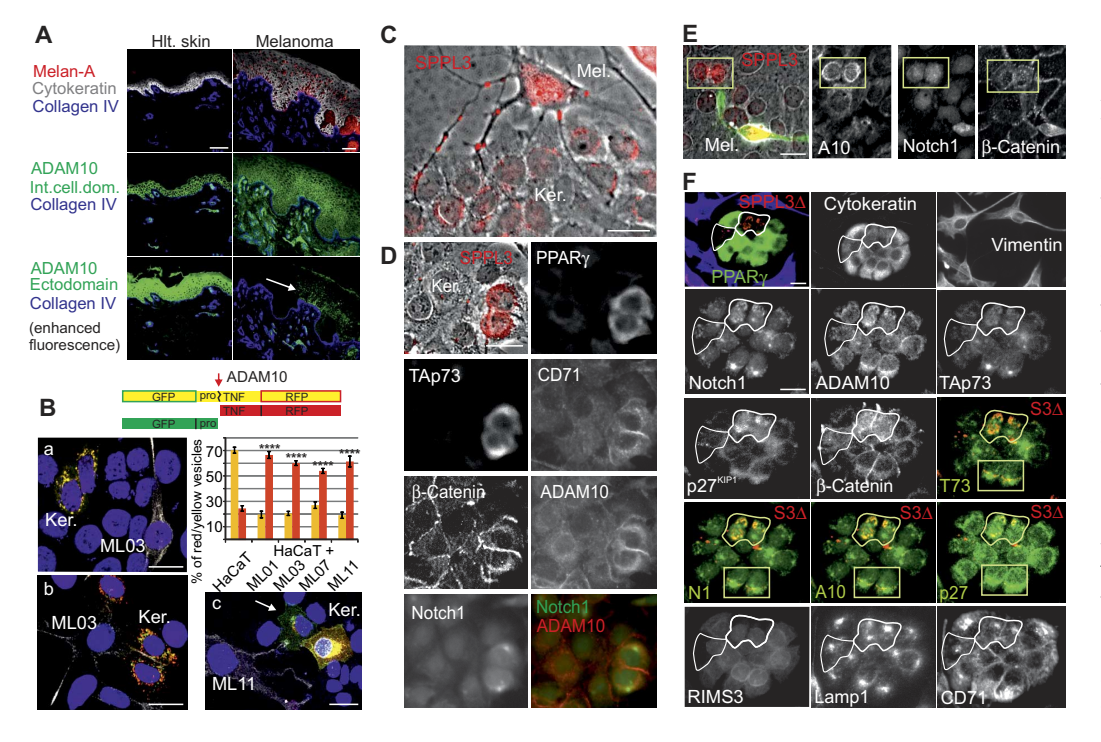


Fig. 4. Melanoma-transferred SPPL3 modulates the keratinocyte PEP and ADAM10 processing. (A) ADAM10 was stained in melanoma- and healthy skin-associated keratinocytes with an antibody recognizing the inhibitory ectodomain (inactive ADAM10; bottom panels) or the C terminus [intracellular domain (int.cell.dom.)]. To demonstrate residual ADAM10 staining (arrow), the fluorescence signal was enhanced (bottom panels). Scale bars, 100 µm. (B) Assessment of the cleavage of G-proTNF-R fusion protein (yellow) in transfected HaCaT cells that either had established contact with melanoma cells ML03 or ML11 (white) (images b and c) or had not (images a and c). Top: Cartoon depicts how cleavage was quantified by counting yellow (proTNF) and red (cleaved, mature TNF) vesicular compartments on one confocal level per cell for 20 randomly selected melanoma-associated cells. Data are means \pm SEM of 20 cells. ****P < 0.0001, compared with HaCaT, one-way analysis of variance (ANOVA) and Dunnett's test. Scale bars, 25 μ m. (\mathbf{C}) Cocultures of mela-

noma cell and keratinocytes were analyzed for factors present in melanoma cell dendrites by MELC using the 57 melanoma antibody panel. The result for SPPL3 is shown. Scale bar, $25 \mu m$. (D) Keratinocytes visibly receiving melanoma cell–derived SPPL3 (upper left) were analyzed for their PEP by MELC. Scale bar, $25 \mu m$. (E) Similar to (D), using a different antibody against Notch1 to demonstrate nuclear Notch1 intracellular domain. Scale bar, $25 \mu m$. (F) Keratinocytes in coculture with ML03 melanoma cells that were transfected with an inactive SPPL3 mutant (SPPL3 Δ) were analyzed for their PEP by MELC. Colocalization of the indicated factors in the presence of transfected SPPL3 Δ or endogenous wild-type SPPL3 is highlighted by outlines or squares, respectively. S3 Δ , SPPL3 Δ ; N1, Notch1; A10, ADAM10; T73, TAp73; p27, p27^{KIP}. Scale bars, 25 μm .

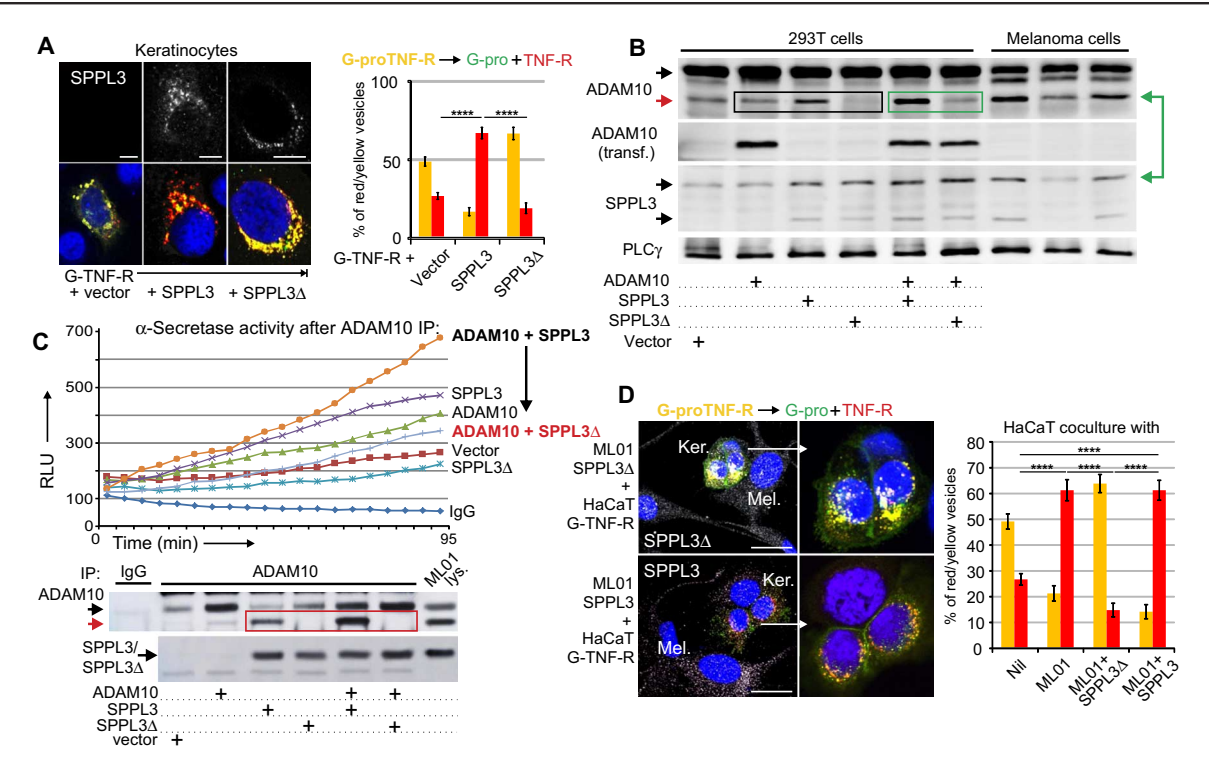


Fig. 5. SPPL3 activates ADAM10. (A) SPPL3 stimulates the (left) confocal imaging of G-proTNF-R processing (red) in 293T cells transfected with adenoviral-packaged SPPL3 or SPPL3 Δ and G-proTNF-R. Cleavage of the fusion protein was quantified as described in Fig. 4B. Data are means ± SEM from 20 cells. ****P < 0.0001, one-way ANOVA and Bonferroni's test. Scale bars, 10 μm. (B) Representative blotting of cell lysates for PLC γ (as a loading control), SPPL3, and total and activated/cleaved (red arrow) ADAM10 in lysates from 293T cells transiently transfected with SPPL3 or SPPL3 Δ and ADAM10 (lanes 1 to 6) or from melanoma cell lines (lanes 7 to 9). Bands boxed in black and green refer to endogenous and transfected ADAM10, respectively. The green arrow points at the ratios of active ADAM10 and SPPL3. (C) Similar to that described in (B), except ADAM10 was immunoprecipitated after 24 hours and analyzed by Western blot (bottom panel), whereas an aliquot was assayed for ADAM10 activity using a commercial α -secretase activity assay (SensoLyte) (top graph). (D) G-proTNF-R processing in HaCaT keratinocytes transfected with G-proTNF-R (yellow) cocultured with SPPL3- or SPPL3 Δ -transfected ML01 melanoma cells. Data are means ± SEM from 20 cells. Scale bars, 25 μm. Nil, not treated or not transfected.

suggest that ADAM10 and not ADAM17 activation may be a crucial event during melanocyte transformation.

SPPL3 is required for ADAM10 activation

Because most of the ADAM10 pool seemed activated in SSM-associated keratinocytes, we assumed that an upstream effector was constantly shuttled into these cells. We tested all 57 melanoma antibodies for recognizing their antigen in cell dendrites in melanoma/keratinocyte cocultures. Two factors were identified, one of which was SPPL3 (Fig. 4C), a family member of intramembrane-cleaving GXGD aspartyl proteases (21), of which, for example, SPPL2a and SPPL2b cooperate with ADAM10 (22, 23).

We first analyzed keratinocytes that received, through dendritic transfer, wild-type SPPL3 or an inactive mutant (SPPL3-D272A; hereafter called SPPL3 Δ) (24) from transfected melanoma cells. Keratinocytes receiving wild-type SPPL3 increased the expression of a number of factors (Fig. 4D). Although Notch1 and ADAM10 did not colocalize, we observed an increased, albeit weak, staining of Notch1 in the nucleus using a different antibody against Notch1 (Fig. 4E). These findings were similar to what we have observed previously in HIV Nef–transfected cells, where we found a role for Notch1 in endosomal trafficking independent of a transcriptional effect (25). Conversely, the transfected SPPL3 mutant blocked the expression of peroxisome proliferator–activated receptor γ (PPAR γ), changed the subcellular distribution of several factors [LAMP1 (lysosomal associated membrane protein 1), RIMS3 (regulating synaptic

membrane exocytosis 3), and CD71], and colocalized with ADAM10, Notch1, TAp73, p27^{KIP}, and β -catenin (Fig. 4F), perhaps through blocking the processing of these proteins or inducing their disposal in lysosomes. Together, these findings suggest that SPPL3 modulated the keratinocyte PEP and was potentially involved in ADAM10 processing.

Supporting this conclusion was our observation that wild-type SPPL3 colocalized with the ADAM10 substrate G-proTNF-R and increased its processing in 293T cells, whereas SPPL3Δ blocked the cleavage (Fig. 5A). Similarly, transfection of SPPL3 into 293T cells activated endogenous ADAM10, whereas SPPL3Δ blocked this process (Fig. 5B, red arrow/black box). The same effect was seen with transfected ADAM10 (green box). Furthermore, in three melanoma cell lines, protein abundance ratios of activated ADAM10 and SPPL3 appeared to be similar (Fig. 5B, green arrow). Finally, both SPPL3 constructs coimmunoprecipitated ADAM10 from transfected 293T cells, but only wild-type SPPL3 associated with the processed (active) ADAM10 form (fig. S6B).

To verify that the proteolytic activity of ADAM10 was dependent on SPPL3, we immunoprecipitated ADAM10 from 293T cells and subjected the protease to a peptide-based activity assay (SensoLyte 520TACE). Transfection of wild-type SPPL3 induced, whereas SPPL3Δ suppressed, ADAM10 protease activity (Fig. 5C). SPPL3 also modulated ADAM10 activity in cocultured keratinocytes; transfection of SPPL3Δ into melanoma cells blocked G-proTNF-R processing in associated keratinocytes (Fig. 5D). Together, these results suggest that SPPL3 is directly involved in the activation of ADAM10.

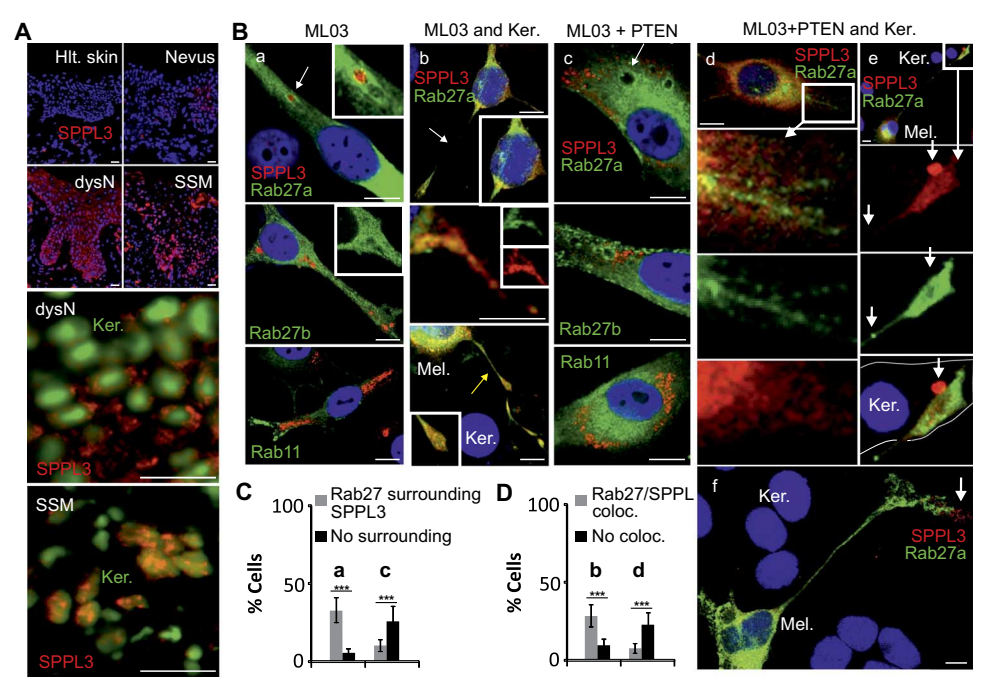


Fig. 6. PTEN modulates the subcellular localization of SPPL3. (A) SPPL3 staining in keratinocytes of healthy (Hlt.) skin, a compound nevus, a dysplastic nevus (dysN), and an SSM (top panel). Close-up image of SPPL3 staining in keratinocytes (green) of a dysplastic nevus and an SSM (bottom panel). Scale bars, 25 μm. (**B**) Confocal imaging of the colocalization of SPPL3 in ML03 cells transfected with Rab27a, Rab27b, or Rab11 (a) and additionally cocultured with keratinocytes (b), cotransfected with PTEN without keratinocyte coculture (c), or cotransfected with PTEN with keratinocyte coculture (d to f). Scale bars, 10 μm. (**C**) Percent of cells in the conditions indicated from (B) showing Rab27a staining around SPPL3. Data are means \pm SEM from 30 cells in three randomly selected visual fields. (**D**) As in (C), with regard to Rab27a and SPPL3 colocalization. ***P < 0.001, one-way ANOVA and Bonferroni's test.

SPPL3 translocation into keratinocytes is modulated by PTEN

Both dysplastic nevi and melanoma cells transferred SPPL3 to keratinocytes (Fig. 6A, top panels, and fig. S7A), but ADAM10 was activated only in melanoma-associated cells. Notably, dysplastic nevi-associated keratinocytes harbored SPPL3 in the cytoplasm, but melanoma-associated cells harbored SPPL3 in the perinuclear/Golgi region (Fig. 6A, bottom panels). In the tissue, no such regulation was observed with SPPL2a or SPPL2b (fig. S7B), and in transfected 293T cells, ADAM10 coprecipitated SPPL3 but not SPPL2a or SPPL2b (fig. S8A).

We therefore analyzed the subcellular localization of SPPL3 in melanoma cells (ML03: BRAF^{V600E+}/PTEN⁻). After transfection of GFP-tagged Rab4, Rab5, Rab7, Rab11, Rab27a, or Rab27b, which are required for the transfer of melanosomes into keratinocytes (26), we found that endogenous SPPL3 was surrounded predominantly by Rab27a and Rab27b (Fig. 6B, arrow in image "a," and fig. S8B). When we cocultured these ML03 cells with keratinocytes, long dendrites developed from melanoma cells and extended to make contact with keratinocytes, and SPPL3 and Rab27a colocalization was visible in small endosomal structures that appeared to be transferred to keratinocytes (Fig. 6B).

Microtubule-associated trafficking of endosomal vesicles is inhibited by PTEN (27), which is frequently inactivated in melanoma cells, including the SSM samples analyzed here (fig. S9) but not in dysplastic nevi (28). Mimicking the situation in dysplastic nevi, we reconstituted PTEN in ML03 cells and coexpressed Rab27a. Under these conditions, SPPL3 was not surrounded by Rab27a (Fig. 6, B and C), and the proteins did not colocalize upon coculture with keratinocytes (Fig. 6, B and D). Unexpectedly, SPPL3 still transferred to keratinocytes (Fig. 6B,

images e and f). In summary, the presence of PTEN inhibited the transfer of SPPL3 via Rab27⁺ endosomes specifically but not its transfer in general. This may explain the cytoplasmic versus perinuclear localization of SPPL3 in dysplastic nevi-associated versus SSM-associated keratinocytes.

PTEN inactivation modulates the PEP in melanomaassociated keratinocytes

To analyze the functional consequences of nonendosomal SPPL3 transfer, we reconstituted PTEN in ML03 melanoma cells and cocultured keratinocytes that expressed G-proTNF-R. In this setting, G-proTNF-R cleavage was blocked (Fig. 7A, images c and d and the associated graph), implying that nonendosomal SPPL3 could not activate or interact with ADAM10. Analyzing the prerequisites for SPPL3/ADAM10 interaction, we found that the down-regulation of PTEN alone by small interfering RNA (siRNA) (fig. S10A) was not sufficient (Fig. 7B, image b). However, overexpression of BRAF^{V600E}, but not wild-type BRAF, induced SPPL3/ADAM10 colocalization (Fig. 7B, image d). This again was abolished after reintroduction of PTEN (Fig. 7B, image e). For confirmation, we analyzed the localization of ADAM10 un-

der these conditions. Only in the presence of BRAF^{V600E} did ADAM10 enter Rab4⁺ and Rab27⁺ endosomes (Fig. 7C, arrow within the images boxed in red), and this effect was blocked in the presence of PTEN. In summary, PTEN counteracted BRAF^{V600E}-stimulated translocation of SPPL3/ADAM10 into the endosomal system.

To demonstrate the functional consequences of this complex regulation, we first analyzed the cleavage of G-proTNF-R. Transient transfections revealed that expression of BRAF V600E was sufficient to activate ADAM10 and cooperated with SPPL3 in G-proTNF-R cleavage (Fig. 7D, conditions boxed in red). Again, expression of PTEN or SPPL3 Δ had the capacity to block this effect. For confirmation, we immunoprecipitated ADAM10 from this experimental setting and assessed its proteolytic activity and presence of cleaved ADAM10. Cotransfection of BRAF V600E and SPPL3 had the strongest effect on the protease activity of ADAM10, assessed as consequential α -secretase activity (Fig. 7E, green line), which correlated with increased abundance of its cleaved form (Fig. 7F, green box; complete experiment and controls shown in fig. S11A) and a prominent coprecipitation of SPPL3 (Fig. 7F, red box). Cotransfection of PTEN and/or SPPL3 Δ blocked the proteolytic activity of ADAM10 (Fig. 7E, conditions labeled with red text), and cotransfections with PTEN blocked the association of ADAM10 with SPPL3 (Fig. 7F, black box).

For further confirmation, we analyzed melanoma cells. In ML03 cells (BRAF $^{V600E+}$, PTEN $^-$) transfection of wild-type BRAF, PTEN, or SPPL3 Δ reduced a preexisting high protease activity (fig. S11B) and blocked the association of ADAM10 with SPPL3 (Fig. 7G, red boxes; complete experiment and controls in fig. S11C). Cotransfection of PTEN or BRAF strongly reduced the protein abundance of ADAM10 (green arrow), potentially explaining the strong inhibitory effects of PTEN.

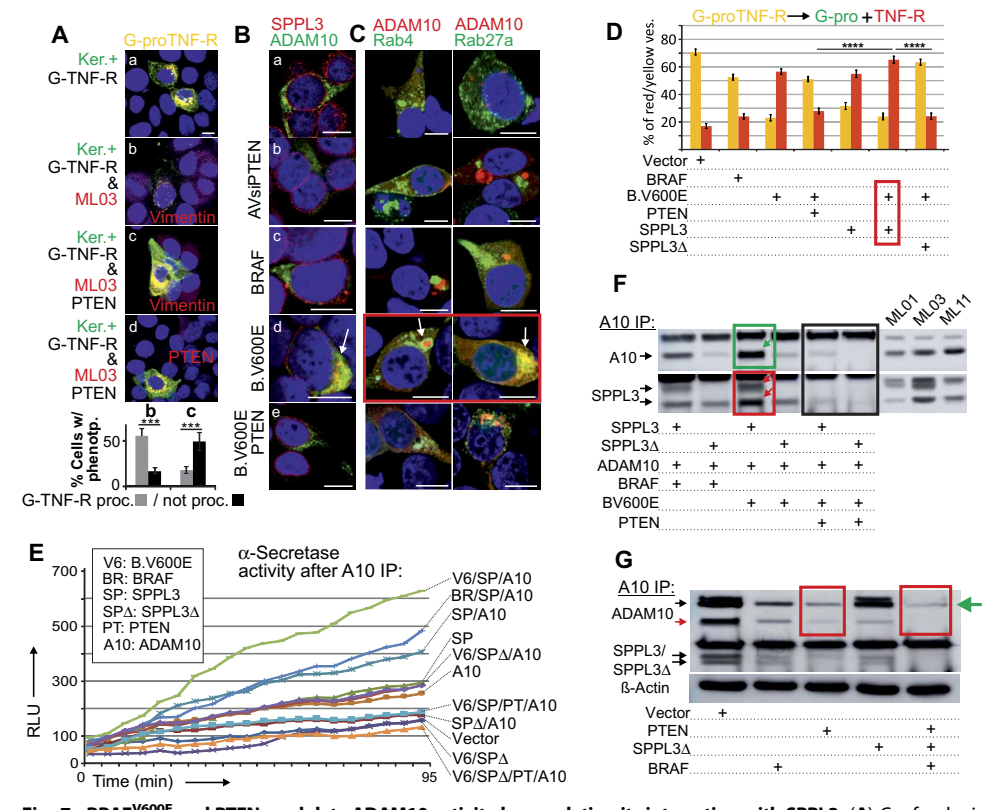


Fig. 7. BRAF^{V600E} and PTEN modulate ADAM10 activity by regulating its interaction with SPPL3. (A) Confocal microscopy assessment of G-proTNF-R processing (reduction of cells with yellow color) in G-proTNF-R-transfected (yellow) keratinocytes (image a) cocultured with control (vector-transfected; image b) or PTEN-transfected (images c and d) melanoma cells (ML03), stained for vimentin (indicating melanoma cells) or PTEN (red). Data in graph are means ± SD from 30 cells in three randomly selected visual fields. Scale bar. 10 um. (B) Confocal microscopy analysis of colocalization of ADAM10 (green) and SPPL3 (red) in 293T cells cotransfected with ADAM10 and SPPL3 (image a) and infected with an adenoviral construct expressing an siRNA for PTEN (AVsiPTEN; fig. S9, image b) or cotransfected with wild-type (image c), BRAF^{V600E} (image d), or BRAF^{V600E} and PTEN (image e). Scale bars, 10 μm. (C) Confocal microscopy analysis of ADAM10 (red) and GFP-Rab4 or GFP-Rab27a (green) colocalization in transfected 293T cells that were additionally cotransfected or infected as in (B). (D) G-proTNF-R processing (counting red and yellow vesicles), analyzed as described in Fig. 5A, in 293T cells cotransfected with G-proTNF-R and additional factors as indicated. The red box depicts the condition leading to colocalization of ADAM10 and Rab4 or Rab27a. Data are means ± SEM from 20 cells in three randomly selected visual fields. ****P < 0.0001, one-way ANOVA and Bonferroni's test. (**E**) α -Secretase activity in ADAM10 immunoprecipitates (A10 IP) from 293T cells cotransfected with the indicated factors. (F) ADAM10 processing (green box and arrow) and SPPL3 coprecipitation (red box and arrows) and blockage of these mechanisms (black box) in ADAM10 immunoprecipitates from 293T cells cotransfected with the indicated factors. For comparison, lysates of melanoma cells were blotted for indicated factors. The whole experiment including controls is shown in fig. S11A. (G) ADAM10 activation and processing and SPPL3 coprecipitation in ADAM10 immunoprecipitates from melanoma cells (MLO3) transfected as indicated. Controls are shown in fig. S11C. Red boxes and green arrow indicate reduced interaction of ADAM10 and SPPL3 and reduced ADAM10 protein abundance, respectively.

Together, these findings support a conclusion that SPPL3 is directly involved in the activation of ADAM10.

Finally, we investigated whether BRAF^{V600E}, SPPL3, and loss of PTEN in primary melanocytes were sufficient to induce a keratinocyte PEP as seen in vivo. To transduce primary melanocytes, adenoviral vectors were established (fig. S10B). One day after infection, melanoma cells were cocultured with keratinocytes, followed 72 hours later with MELC analysis. Each factor by itself had an effect on the keratinocyte PEP; however, expression of BRAF^{V600E}, SPPL3, and siRNA against *PTEN* together produced the highest abundance of a panel of eight proteins (Fig. 8), resembling the PEP of keratinocytes surrounding SSMs (Fig. 2D). Overall, this experiment appeared to recapitulate the stepwise increase in protein abundance seen in keratinocytes in vivo, from benign nevi to SSM (Fig. 3).

DISCUSSION

Our data indicate that the early transformation process of the most common form of cutaneous melanoma involves the activation of ADAM10 in a stepwise and SPPL3dependent manner. Although we analyzed only six early BRAF $^{V600E+}$ SSMs, our previous report on the activation of ADAM10 in 30 of 31 primary melanoma lines supports our conclusion. This report places ADAM10 activation into the context of early melanoma development, which seemingly differs from classical views, assuming a stimulation of cell proliferation and survival downstream of ERK1/2 (29, 30). However, because we also found an increased presence of phosphorylated ERK1/2 in our tissue analysis, we envision our results as an extension of current models. Surprisingly, we found that more variables were involved in melanocyte transformation than appreciated so far, including protein abundance, their subcellular localization, and potentially the early keratinocyte environment. Keratinocytes with an altered PEP may stimulate transforming melanocytes, similar as they stimulate melanin production after sun exposure. The reciprocal transfer of new effectors may occur through cell-cell contact and cell dendrites or alternatively through endosomal secretion (25) or transcytosis (31). Although we have no direct proof for such a reciprocal cell interaction, such a scenario would be consistent with the often slow changes seen in premalignant melanocytic lesions.

The so far little analyzed protease and presenilin homolog SPPL3 turned out to be a key factor in ADAM10 activation. Because furin is believed to cleave ADAM10 (32, 33), the control of protein glycosylation by SPPL3 (34) may have a critical role in ADAM10 activation. As described for ADAM17, glycosylation plays an essential role in the regulated activation of this pro-

tease class (35). A more detailed analysis was beyond the scope of this report but is necessary to detail the precise role of SPPL3 in ADAM10 activation.

From a general perspective, the activation of key proteases in a cancer cell seems plausible because this may (i) allow autonomous cell proliferation through modulation of cell adhesion and cleavage of extracellular matrix and (ii) stimulate signaling pathways through the cleavage of inactive precursor proteins. In the following, we first delineate molecular steps that are potentially involved in the melanocyte transformation process and then outline a possible sequel of events.

We found that 26 of 31 of primary melanoma lines harbored tyrosinephosphorylated paxillin and assumed that ADAM10 is activated in an integrin/paxillin-dependent manner (10). Supporting this conclusion is the observation that integrins are commonly activated in melanoma cells (36). Paxillin is a scaffold protein for the RAF/MEK/ERK1/2 signaling

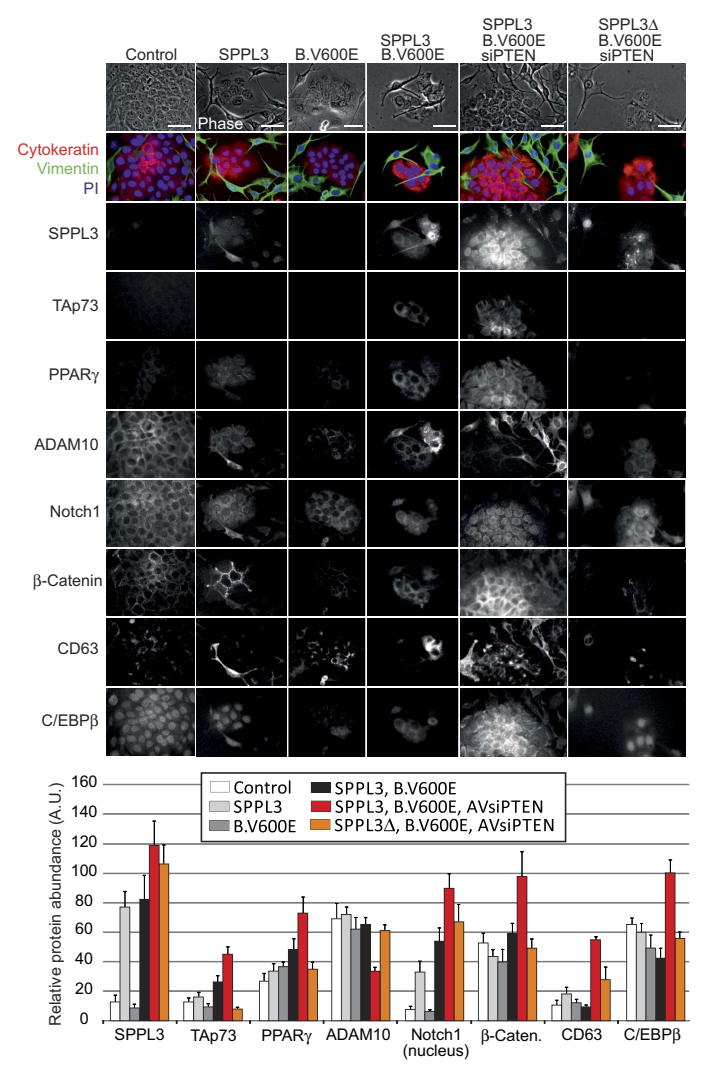


Fig. 8. BRAF^{V600E}, SPPL3, and knockout of *PTEN* in melanocytes induce the melanoma-associated keratinocyte PEP. Primary melanocytes were infected with adenoviral constructs expressing the indicated factors and a *PTEN*-targeted siRNA (expression controls in fig. S10). Twenty-four hours later, a few keratinocytes were seeded in between the transfected melanocytes to form little colonies. After an additional 48 hours of culture, the cocultures were washed, fixed, and analyzed by MELC for the indicated factors. Relative protein abundance was determined in the different colonies (as in fig. S3) by assessing the gray value intensity per cell, similar to that described in Fig. 1B. Data are means \pm SEM from five different colonies. Scale bars, 50 μ m.

module (*37*); thus, BRAF^{V600E} may stimulate the activation of ADAM10 as well as ERK1/2 by a paxillin/integrin complex. In concert with growth factors, integrins are able to initiate the cell cycle (*38*, *39*). This was demonstrated in melanocytes, is characterized by cyclin D1 up-regulation and p27^{KIP1} down-regulation, and is seemingly bypassed by BRAF^{V600E} in melanoma cells (*40*). We envision a mechanism whereby ADAM10 and BRAF^{V600E} override cell cycle suppression that is enforced by cell adhesion and the requirement for growth factor stimulation (fig. S12A).

The increased abundance of β -catenin and altered subcellular localization were prominent findings in our analysis, and the relevance of this pathway in melanoma is well documented (41, 42). This may, in part, explain why the abundance of many factors was increased in melanoma cells relative to nevi and healthy skin. We would speculate that β -catenin

is activated by epidermal growth factor receptor (EGFR) stimulation, induced by ADAM10 cleavage of the EGFR ligand (fig. S12B). This is a well-described function of ADAM10 and has an important role in breast cancer progression (43). EGF stimulation of EGFR induces CK2 activation, which was increased in our study (Figs. 2 and 3) and liberates β -catenin from its association with α -catenin and E-cadherin (44). Moreover, the presence of BRAF could stimulate this pathway directly (fig. S12B). Finally, the here detected Notch1 receptor cleavage, which we assume is caused by its canonical activator ADAM10, correlates with melanoma progression (45). Notably, a recent report found that Notch1 cleavage is triggered by the interaction of melanoma cells with keratinocytes (46). In summary, an early melanoma transformation process may involve ADAM10 at a critical junction.

Mutation of BRAF is likely the first step in many melanocyte transformations (47). Thereafter, general protein abundance in melanocytes and keratinocytes may increase steadily, including that of SPPL3. Potentially, the melanocyte-keratinocyte reciprocal interaction augments this effect (fig. S12C). In some cases, this may continue through different stages of nevi, as reflected by their changing PEPs (Fig. 3), until a dysplastic nevus or, with additional mutations (28), an early horizontally growing in situ melanoma has developed. At least in a defined subset of cutaneous melanomas, a critical step toward full transformation occurs when PTEN is inactivated (9). This allows BRAFV600E to shuttle SPPL3 and ADAM10 into endosomal compartments (fig. S12D). The interaction of both factors may occur mainly in Rab4⁺ and Rab27⁺ endosomes (Fig. 7, C and D), leading to high concentrations of activated ADAM10. Perhaps this induces the cleavage of additional precursor proteins present in endosomal compartments. In addition, active ADAM10 is secreted in extracellular vesicles (10), stimulating the early melanoma microenvironment in an autocrine and paracrine fashion. In the event that a mutation in PTEN or another with equivalent consequence is induced before a BRAF mutation occurs, we would expect a more rapid development of melanoma from seemingly unaffected skin. Such a scenario seems plausible given that many mutations accumulate over time in healthy skin (15). Additional studies should show whether the mechanism presented here is induced by mutations other than BRAF^{V600E} and in PTEN.

Our insights here into the early melanoma transformation events were obtained through a multiantigen assessment in tissue. The topographical allocation of PEPs was key to our approach and a major difference to other multiantigen approaches, such as mass spectrometry. Knowing the most important driver mutations in early melanomas enabled us to validate our findings. We therefore conclude that systemic approaches on both the protein and genome levels are necessary to get a better insight into cancer development. Furthermore, the protein markers demonstrated in this study, particularly in melanoma-associated keratinocytes, could be used for the diagnosis of early melanomas and the discrimination of dysplastic lesions from truly transformed melanocytes.

MATERIALS AND METHODS

Tissue samples

Healthy tissue and tumor samples from patients were obtained immediately after surgery from the Department of Dermatology, University Hospital Erlangen, after approval of the local ethics committee. One part of the sample was embedded in Tissue-Tek O.C.T. Compound (Sakura Finetek) and cryopreserved at -80° C for the MELC analyses, and the remainder was fixed by paraformaldehyde (PFA) for regular histopathological diagnosis.

Cell lines and cell culture

Melanoma cell lines (ML01, ML03, ML05, ML07, and ML11) were described recently and generated from fresh tumor biopsies obtained directly after surgery. A single-cell suspension was produced by mechanical dissociation and enzymatic digestion with deoxyribonuclease and collagenase. Cells were seeded in RPMI supplemented with 20% human serum into six-well plates. Passaging of cells was performed according to cell density. ML01 and ML03 were selected for many experiments because of their mutation profile (BRAF^{V600E+} PTEN⁻), large cell size, and growth behavior in vitro. Primary human epidermal melanocytes were purchased from PromoCell and cultured in melanocyte growth medium provided according to the manufacturer's procedures. 293T/ HaCaT cells were cultured in Dulbecco's modified Eagle's medium/ RPMI (Lonza), 10% (v/v) fetal bovine serum with penicillin-streptomycin. Coculture experiments of melanoma cells/primary melanocytes and HaCaT were performed as described by (48) with a seeding ratio of 1:5. All cells were grown at 37°C under 5% CO₂.

Immunohistochemistry

For immunohistochemistry staining, formalin-fixed paraffin-embedded samples were deparaffinized and antigen retrieval was achieved in tris-EDTA buffer (pH 9) for 30 min at 100°C. For antigen detection, the LSAB method (Dako REAL Detection Systems) was used, performed by the Dako Autostainer Plus.

MELC sample preparation

Tissue sections of $5\,\mu m$ were prepared using a cryotome (Leica CM3050 S), incubated in acetone (Carl Roth) for 10 min at -20° C, and air-dried for 5 min. For rehydration, the slides were placed in phosphate-buffered saline (PBS; PAA) for 5 min at room temperature, followed by incubation with 5% normal goat serum (Dako) in PBS for 30 min to block unspecific binding sites.

MELC antibody library

For MELC analyses, fluorophore-labeled antibodies and propidium iodide (Genaxxon bioscience) were used (see list of antibodies below). If necessary, antibodies were labeled with fluorescein isothiocyanate (FITC) using the Pierce FITC Antibody Labeling Kit from Thermo Fisher Scientific and tested again after labeling using melanoma tissue samples. The best working dilutions of the antibodies for the MELC analysis were determined in initial calibration runs, adjusted if necessary, and tested again.

MELC data generation

The MELC technology has been described previously (18). The coverslip with the sample was positioned onto a motor-controlled xy stage of an inverted fluorescence microscope (Leica DMIRE2, Leica Microsystems; ×20 air lens; numerical aperture, 0.7). The repetitive cyclic process of this method includes the flowing steps: (i) antigen tagging by a fluorescence-coupled monoclonal antibody, (ii) washing, (iii) image assessment, and (iv) photobleaching. By means of a pipetting robot unit, the antibodies were incubated with the sample for 30 min and subsequently rinsed with PBS. Phase contrast and fluorescence signal were assessed by a cooled charge-coupled device camera (Apogee KX4, Apogee Instruments). The photobleaching step at the excitation wavelengths was connected downstream the washing steps. After completion of the cycle, the next antibody was added to the same tissue sample. Two to four visual fields were recorded simultaneously during each MELC run. Data acquisition was achieved using imaging software developed by the

former company MelTec GmbH. For quantification and calculation of signal intensity, the ROI (regions of interest) manager tool of the ImageJ software was used.

MELC data analysis

With the corresponding phase-contrast images, fluorescence images produced after each antibody stain were aligned pixel-wise and were corrected for illumination faults using flat-field correction. The alignment reached a resolution of ± 1 pixel. Postbleaching images were subtracted from the following fluorescence tag images. Superimposed images composed an n epitope presence in relation to each pixel (900 \times 900 nm² area) of a visual field (1024 \times 1024 pixels). After the MELC staining procedure, the relative expression level of an antigen was determined in 6 to 30 tissue areas (see example in fig. S3) by assessing the gray value intensity relative to the background. The scale bar represents 100 μm . Values were obtained using the following equation:

$$RFI(AG)_X = \frac{\sum_{i=1}^{n} MGV(AG)_i}{n} - \frac{\sum_{j=1}^{m} IntDen(BG)_j}{\sum_{j=1}^{m} A_j}$$

where RFI is the relative fluorescence intensity, AG is antigen, MGV is the mean gray value, IntDent is the integrated density, and BG is background.

Immunocytochemistry

For immunocytochemistry analyses, cells were cultured on glass slides for 2 hours at 37°C and subsequently fixed by 3% PFA for 30 min at room temperature, followed by three washes with PBS/1% bovine serum albumin (BSA). Cells were then permeabilized with 0.1% Triton X-100/1% BSA and immunostained by standard procedures (primary and secondary antibodies). Finally, the cells were washed for 30 min with PBS/1% BSA and mounted with Fluoromount-G (SouthernBiotech). Slides were analyzed on a Zeiss laser scanning microscope LSM780 equipped with the ZEN software (Carl Zeiss AG).

DNA constructs and transfection

For transient transfections, 293T, melanoma, and HaCaT cells were transfected with Lipofectamine LTX with PLUS Reagent (Invitrogen) according to the manufacturer's instructions or by using the calcium phosphate procedure. Cells were, in general, analyzed 24 to 72 hours after transfection. Rab-GFP (4, 5, 7, 11, 27a, and 27b) were constructed by overlapping polymerase chain reaction (PCR)-based cloning technique. G-proTNF-R was described recently in (10). SPPL3 and SPPL3 Δ were obtained by R. Fluhrer [German Center for Neurodegenerative Diseases (DZNE), Munich, Germany] (22, 23). BRAF and PTEN were purchased from Addgene and cloned into the pEF-BOS expression vector (Addgene). BRAF^{V600E} mutation was inserted using the QuikChange II Site-Directed Mutagenesis Kit (Agilent) according to the manufacturer's instructions using the following primers: t58a-sense (5'-attttggtctagctacagagaaatctcgatggagtgg-3') and t58a-antisense (3'-taaaaccagatcgatgtctctttagagctacctcacc-5'). Successful mutagenesis was confirmed by Sanger sequencing.

Adenoviral constructs and transduction

The PTEN siRNA sequence (5'-CAAGAUCUUCACAAAAGGGUU-3') (49) was cloned upstream a U6 promoter region into a commercially available adenoviral vector system from Eurofins Genomics, containing a cytomegalovirus (CMV) promoter–controlled GFP expression cassette. Similarly, BRAF, BRAF V600E , SPPL3, and SPPL3 Δ were introduced

into the pShuttle CMV vector of the AdEasy-1 vector system (Addgene). Resulting recombinant replication-deficient serotype 5–derived adenoviruses were amplified in 293 cells. All viruses were purified by two rounds of cesium chloride equilibrium density gradient ultracentrifugation. Verification of adenovirus preparations and exclusion of wild-type contamination were performed by PCR. Expression of proteins was verified by GFP expression and Western blot as demonstrated in fig. S9. Physical particle concentration [viral particles (vp)/ml] was determined by $\rm OD_{260}$ (optical density at 260 nm) reading; infectious particle concentration was determined by $\rm TCID_{50}$ (median tissue culture infectious dose) assay on 293 cells.

Immunoprecipitation

Cell lysates (500 $\mu g)$ were incubated with 2 μg of primary antibody overnight at 4°C. Afterward, 25 μl of protein G beads (50% bead slurry; GE healthcare) was added into the sample and incubated for 2 hours at 4°C. Subsequently, samples were washed three times with lysis buffer. Supernatants were removed, and beads were boiled for 5 min at 95°C with twofold SDS-loading buffer. Samples were analyzed by standard Western blotting.

Western blot

Proteins separated by SDS-polyacrylamide gel electrophoresis were transferred onto nitrocellulose filters (Schleicher & Schuell) with a pore size of 0.2 µm with the wet blotting device Mini-Protean II Cell and System (Bio-Rad) at 400 mA for 45 min. Subsequently, the filters were blocked with blocking buffer for 1 hour at room temperature to prevent unspecific binding of the antibody. After three successive washes with distilled water, primary antibody diluted 1:500 to 1:5000 in TBS/Tween 20 was added and incubated for 1 hour (room temperature) or overnight (4°C). Thereafter, filters were washed three times for 5 min with PBS/0.02% Tween 20 before they were incubated for 1 hour at 4°C with the corresponding secondary horseradish peroxidase-conjugated antimouse or anti-rabbit antibody diluted 1:2000 to 1:5000 in PBS/0.02% Tween 20. Finally, the filters were washed three times for 10 min with PBS/0.02% Tween 20 before the antibody/enzyme complexes were visualized by enhanced chemiluminescence (Pierce) according to the manufacturer's instructions.

lpha-Secretase activity assay

The assay was performed essentially as described previously (10) using a commercial, SensoLyte 520 α -Secretase Activity Assay Kit (AnaSpec 72085), according to the manufacturer's instructions. Briefly, we placed immunoprecipitated samples (the equivalent of 1-ml plasma) on a 96-well black flat-bottom plate (Greiner 655900) and added a 5-FAM (fluorophore) and QXL 520 (quencher)–labeled fluorescence resonance energy transfer (FRET) peptide substrate for continuous measurement of enzyme activity. Upon cleavage of the FRET peptide by the active enzyme, the fluorescence of 5-FAM is recovered and continuously monitored at an excitation of 490 nm and emission of 520 nm by a preheated (37° C) TECAN infinite M200 Pro plate reader.

Antibody screening and purification

The antibody facility at the Institute of Molecular Immunology, Helmholtz Center Munich, an institution financed by the German government, produces antibodies in collaboration with research groups in Germany, aiming to support research. All antibodies, which are generated by peptide immunization, are owned by the Helmholtz Center and provided for research purposes. Hence, their antibody stock reflects the

research activities in Germany. We asked the Helmholtz Center Munich to provide 1000 randomly selected and pretested [tested by enzymelinked immunosorbent assay (ELISA) against the primary peptide used for immunization] antibodies/hybridomas from their stock. From these 1000 antibodies, 814 were eventually screened as outlined in fig. S1. Antibodies staining epidermal and dermal melanoma cells and not staining nevi or other tissue (n = 57), antibodies staining only keratinocytes (n =7), and antibodies staining keratinocytes and melanoma cells (n = 19)(see list of antibodies in table S1) were amplified and purified by the Helmholtz Center Munich. They were subsequently labeled with FITC using a commercial labeling kit (Pierce FITC Antibody Labeling Kit, Thermo Fisher Scientific) and tested again on melanoma tissue by MELC. The following purified antibodies were finally provided by the Helmholtz Center Munich: α -ABPP, α -ADAM10, α -AGO2, α -APBB1, α-BOP1, α-C/EBPα, α-CK2A2, α-CPEB3, α-CXorf22, α-DP103, α-p-EBF3, α-GBA2, α-GBP1, α-GTP, cyclohyd.-1, α-H2B-Ub, α-p-LRP6, α-MECP2, α-NRG1, α-ORC3, α-p2 7^{KIP1} , α-PCNA, α-p-RNAP II, α-RNase III, α-RIMS3, α-SFRP2, α-Sirtuin-2, α-SPPL3, α-synuclein, α -SYT10, α -TAp73, α -TCR, α -TMEM147, α -TRAF1, and α -UHRF2.

Antibodies from commercial providers for experiments and MELC analysis (see also table S1)

Additional antibodies were purchased from the following suppliers: Abcam: α-ADAM10, α-cytokeratin-14-FITC, α-myc, α-Notch1-FITC, α-activated Notch1 (ab8925), and α-tyrosinase-FITC; Abgent: α -SPPL3; BD Pharmingen: α -CD71-FITC, α -E-cadherin-FITC, α-LAMP1-FITC, and α-Rac-1-FITC; Beckman Coulter: α-CD25-FITC, α -HLA-ABC-FITC, and α -HLA-DR-FITC; BioLegend: α-CD63-FITC; Biomol: α-collagen IV-FITC and α-PTEN-FITC; Cell Signaling Technology: α -p-ERK1/2-Alexa Fluor 488 and α -PLC α ; Dako: α -Bcl-2-FITC, α -CD68-FITC, α -PTEN, and α -vimentin; eBioscience: α-MCAM-FITC and α-nestin-Alexa Fluor 488; GeneTex: α-PTEN; Life Technologies: α-Ki67–FITC and α-mouse–Alexa Fluor 555; Miltenyi Biotec: α-CD36-FITC, α-CD66abce-FITC, α-CD86-FITC, and α -IFN-FITC; R&D Systems: α -ADAM10-FITC, α - β -catenin-FITC, and α-TACE-FITC; Santa Cruz Biotechnology: α-BRAF-FITC, α-p-connexin 43-FITC, α-Melan-A-FITC, α-PPARα-FITC, α-TRAIL-FITC, and α-vimentin-FITC; Sigma-Aldrich: α-flag; and Zytomed Systems: α -BRAF^{V600E}.

ADAM10 antibody generation

The ADAM10 antibody against the C-terminal domain was generated by the Institute of Molecular Immunology, Helmholtz Center Munich, immunizing mice with a synthesized peptide and applying the conventional hybridoma technology. The peptide sequence selection from the C-terminal domain of ADAM10 (AA704 PSSNPKLPPPKPLC AA716) as well as the peptide synthesis were performed by the Peptide Specialty Laboratories GmbH, Heidelberg. Resulting hybridomas were screened for reactivity with the immunizing peptide by ELISA and further tested by immunohistochemistry using healthy skin and melanoma tissue.

Statistical analysis

GraphPad Prism and Microsoft Excel software were used for statistical analysis (one- and two-way ANOVA and Bonferroni's and Dunnett's test for multiple comparison tests).

SUPPLEMENTARY MATERIALS

www.sciencesignaling.org/cgi/content/full/10/470/eaai8288/DC1 Fig. S1. Screening algorithm to obtain melanoma-specific antibodies.

- Fig. S2. BRAF^{V600E} staining of melanoma tissue.
- Fig. S3. Assessment of relative protein expression levels after MELC analysis.
- Fig. S4. Melanoma- but not nevi-associated keratinocytes have an altered PEP, and an enhanced fluorescence signal reveals nuclear Notch1 staining.
- Fig. S5. Tissue sections of different nevi and SSM growth phases analyzed by MELC.
- Fig. S6. Quantification of the keratinocyte PEP in healthy skin, different nevi, and SSM and coimmunoprecipitation of ADAM10 with SPPL3.
- Fig. S7. Expression of SPPL3, SPPL2a, and SPPL2b in keratinocytes associated with healthy skin, nevi. and SSM.
- Fig. S8. Coimmunoprecipitation of the SPPL3 but not SPPL2a or SPPL2b with ADAM10 and subcellular localization of SPPL3 in melanoma cells.
- Fig. S9. Abundance of PTEN in SSM, healthy skin, and a dysplastic nevus.
- Fig. S10. Expression control of adenoviral constructs in primary melanocytes.
- Fig. S11. $\textsc{BRAF}^{\text{V}600E}$ and PTEN modulate ADAM10 activity in melanoma cells.
- Fig. S12. Hypothetical model on the activation and role of ADAM10 in melanocyte transformation.
- Table S1. List of antibodies used for MELC analysis.
- Table S2. Melanoma-associated keratinocytes change their PEP.

REFERENCES AND NOTES

- E. Hodis, I. R. Watson, G. V. Kryukov, S. T. Arold, M. Imielinski, J.-P. Theurillat, E. Nickerson, D. Auclair, L. Li, C. Place, D. DiCara, A. H. Ramos, M. S. Lawrence, K. Cibulskis, A. Sivachenko, D. Voet, G. Saksena, N. Stransky, R. C. Onofrio, W. Winckler, K. Ardlie, N. Wagle, J. Wargo, K. Chong, D. L. Morton, K. Stemke-Hale, G. Chen, M. Noble, M. Meyerson, J. E. Ladbury, M. A. Davies, J. E. Gershenwald, S. N. Wagner, D. S. B. Hoon, D. Schadendorf, E. S. Lander, S. B. Gabriel, G. Getz, L. A. Garraway, L. Chin, A landscape of driver mutations in melanoma. *Cell* 150, 251–263 (2012).
- Cancer Genome Atlas Network, Genomic classification of cutaneous melanoma. Cell 161, 1681–1696 (2015).
- B. C. Bastian, A. B. Olshen, P. E. LeBoit, D. Pinkel, Classifying melanocytic tumors based on DNA copy number changes. Am. J. Pathol. 163, 1765–1770 (2003).
- J. Bauer, B. C. Bastian, Distinguishing melanocytic nevi from melanoma by DNA copy number changes: Comparative genomic hybridization as a research and diagnostic tool. *Dermatol. Ther.* 19, 40–49 (2006).
- P. M. Pollock, U. L. Harper, K. S. Hansen, L. M. Yudt, M. Stark, C. M. Robbins, T. Y. Moses, G. Hostetter, U. Wagner, J. Kakareka, G. Salem, T. Pohida, P. Heenan, P. Duray, O. Kallioniemi, N. K. Hayward, J. M. Trent, P. S. Meltzer, High frequency of *BRAF* mutations in nevi. *Nat. Genet.* 33, 19–20 (2003).
- P. Uribe, I. I. Wistuba, S. González, BRAF mutation: A frequent event in benign, atypical, and malignant melanocytic lesions of the skin. Am. J. Dermatopathol. 25, 365–370 (2003).
- T. Bogenrieder, M. Herlyn, The molecular pathology of cutaneous melanoma. Cancer Biomark. 9, 267–286 (2010).
- B. C. Bastian, The molecular pathology of melanoma: An integrated taxonomy of melanocytic neoplasia. Annu. Rev. Pathol. 9, 239–271 (2014).
- D. Dankort, D. P. Curley, R. A. Cartlidge, B. Nelson, A. N. Karnezis, W. E. Damsky Jr., M. J. You, R. A. DePinho, M. McMahon, M. Bosenberg, Braf^{V600E} cooperates with *Pten* loss to induce metastatic melanoma. *Nat. Genet.* 41, 544–552 (2009).
- J.-H. Lee, S. Wittki, T. Bräu, F. S. Dreyer, K. Krätzel, J. Dindorf, I. C. D. Johnston, S. Gross, E. Kremmer, R. Zeidler, U. Schlötzer-Schrehardt, M. Lichtenheld, K. Saksela, T. Harrer, G. Schuler, M. Federico, A. S. Baur, HIV Nef, Paxillin, and Pak1/2 regulate activation and secretion of TACE/ADAM10 proteases. *Mol. Cell* 49, 668–679 (2013).
- J. M. Brandner, N. K. Haass, Melanoma's connections to the tumour microenvironment. Pathology 45, 443–452 (2013).
- C. C. Naus, D. W. Laird, Implications and challenges of connexin connections to cancer. Nat. Rev. Cancer 10, 435–441 (2010).
- A. B. Glick, S. H. Yuspa, Tissue homeostasis and the control of the neoplastic phenotype in epithelial cancers. Semin. Cancer Biol. 15, 75–83 (2005).
- G. S. Goldberg, P. D. Lampe, B. J. Nicholson, Selective transfer of endogenous metabolites through gap junctions composed of different connexins. *Nat. Cell Biol.* 1, 457–459 (1999).
- I. Martincorena, A. Roshan, M. Gerstung, P. Ellis, P. Van Loo, S. McLaren, D. C. Wedge, A. Fullam, L. B. Alexandrov, J. M. Tubio, L. Stebbings, A. Menzies, S. Widaa, M. R. Stratton, P. H. Jones, P. J. Campbell, High burden and pervasive positive selection of somatic mutations in normal human skin. *Science* 348, 880–886 (2015).
- N. K. Haass, D. Ripperger, E. Wladykowski, P. Dawson, P. A. Gimotty, C. Blome, F. Fischer, P. Schmage, I. Moll, Johanna M. Brandner, Melanoma progression exhibits a significant impact on connexin expression patterns in the epidermal tumor microenvironment. *Histochem. Cell Biol.* 133, 113 (2010).

- M. Hsu, T. Andl, G. Li, J. L. Meinkoth, M. M. Herlyn, Cadherin repertoire determines partner-specific gap junctional communication during melanoma progression. *J. Cell Sci.* 113 (Pt. 9), 1535–1542 (2000).
- W. Schubert, B. Bonnekoh, A. J. Pommer, L. Philipsen, R. Böckelmann, Y. Malykh, H. Gollnick, M. Friedenberger, M. Bode, A. W. M. Dress, Analyzing proteome topology and function by automated multidimensional fluorescence microscopy. *Nat. Biotechnol.* 24, 1270–1278 (2006).
- W. H. Clark Jr., A. M. Ainsworth, E. A. Bernardino, C.-H. Yang, M. C. Mihm Jr., R. J. Reed, The developmental biology of primary human malignant melanomas. Semin. Oncol. 2, 83–103 (1975).
- 20. J. Schlondorff, J. D. Becherer, C. P. Blobel, Intracellular maturation and localization of the tumour necrosis factor α convertase (TACE). *Biochem. J.* **347** (Pt. 1), 131–138 (2000).
- M. Voss, B. Schröder, R. Fluhrer, Mechanism, specificity, and physiology of signal peptide peptidase (SPP) and SPP-like proteases. *Biochim. Biophys. Acta* 1828, 2828–2839 (2013).
- L. Martin, R. Fluhrer, K. Reiss, E. Kremmer, P. Saftig, C. Haass, Regulated intramembrane proteolysis of Bri2 (ltm2b) by ADAM10 and SPPL2a/SPPL2b. J. Biol. Chem. 283, 1644–1652 (2008).
- V. Kirkin, N. Cahuzac, F. Guardiola-Serrano, S. Huault, K. Lückerath, E. Friedmann, N. Novac, W. S. Wels, B. Martoglio, A.-O. Hueber, M. Zörnig, The Fas ligand intracellular domain is released by ADAM10 and SPPL2a cleavage in T-cells. *Cell Death Differ.* 14, 1678–1687 (2007).
- R. Fluhrer, C. Haass, Signal peptide peptidases and gamma-secretase: Cousins of the same protease family? Neurodegener. Dis. 4, 112–116 (2007).
- C. Ostalecki, S. Wittki, J.-H. Lee, M. M. Geist, N. Tibroni, T. Harrer, G. Schuler, O. T. Fackler, A. S. Baur, HIV Nef- and Notch1-dependent endocytosis of ADAM17 induces vesicular TNF secretion in chronic HIV infection. EBioMedicine 13, 294–304 (2016).
- M. Strom, A. N. Hume, A. K. Tarafder, E. Barkagianni, M. C. Seabra, A family of Rab27binding proteins. Melanophilin links Rab27a and myosin Va function in melanosome transport. J. Biol. Chem. 277, 25423–25430 (2002).
- A. Naguib, G. Bencze, H. Cho, W. Zheng, A. Tocilj, E. Elkayam, C. R. Faehnle, N. Jaber, C. P. Pratt, M. Chen, W.-X. Zong, M. S. Marks, L. J. Tor, D. J. Pappin, L. C. Trotman, PTEN functions by recruitment to cytoplasmic vesicles. *Mol. Cell* 58, 255–268 (2015).
- 28. A. H. Shain, B. C. Bastian, From melanocytes to melanomas. *Nat. Rev. Cancer* **16**, 345–358 (2016)
- K. S. Smalley, A pivotal role for ERK in the oncogenic behaviour of malignant melanoma? Int. J. Cancer 104, 527–532 (2003).
- P. Lopez-Bergami, The role of mitogen- and stress-activated protein kinase pathways in melanoma. Pigment Cell Melanoma Res. 24, 902–921 (2011).
- M. González-Gaitán, Signal dispersal and transduction through the endocytic pathway. Nat. Rev. Mol. Cell Biol. 4, 213–224 (2003).
- A. Anders, S. Gilbert, W. Garten, R. Postina, F. Fahrenholz, Regulation of the α-secretase ADAM10 by its prodomain and proprotein convertases. FASEB J. 15, 1837–1839 (2001).
- T. Kang, Y.-G. Zhao, D. Pei, J. F. Sucic, Q.-X. Sang, Intracellular activation of human adamalysin 19/disintegrin and metalloproteinase 19 by furin occurs via one of the two consecutive recognition sites. J. Biol. Chem. 277, 25583–25591 (2002).
- M. Voss, U. Künzel, F. Higel, P.-H. Kuhn, A. Colombo, A. Fukumori, M. Haug-Kröper, B. Klier, G. Grammer, A. Seidl, B. Schröder, R. Obst, H. Steiner, S. F. Lichtenthaler, C. Haass, R. Fluhrer, Shedding of glycan-modifying enzymes by signal peptide peptidase-like 3 (SPPL3) regulates cellular N-glycosylation. *EMBO J.* 33, 2890–2905 (2014).
- C. Adrain, M. Zettl, Y. Christova, N. Taylor, M. Freeman, Tumor necrosis factor signaling requires iRhom2 to promote trafficking and activation of TACE. Science 335, 225–228 (2012).
- S. Kuphal, R. Bauer, A.-K. Bosserhoff, Integrin signaling in malignant melanoma. Cancer Metastasis Rev. 24, 195–222 (2005).
- W. Kolch, Coordinating ERK/MAPK signalling through scaffolds and inhibitors. Nat. Rev. Mol. Cell Biol. 6, 827–837 (2005).
- X. Zhu, M. Ohtsubo, R. M. Böhmer, J. M. Roberts, R. K. Assoian, Adhesion-dependent cell cycle progression linked to the expression of cyclin D1, activation of cyclin E-cdk2, and phosphorylation of the retinoblastoma protein. J. Cell Biol. 133, 391 (1996).
- A. Mettouchi, S. Klein, W. Guo, M. Lopez-Lago, E. Lemichez, J. K. Westwick,
 F. G. Giancotti, Integrin-specific activation of Rac controls progression through the G₁ phase of the cell cycle. *Mol. Cell* 8, 115–127 (2001).
- K. V. Bhatt, L. S. Spofford, G. Aram, M. McMullen, K. Pumiglia, A. E. Aplin, Adhesion control of cyclin D1 and p27^{Kip1} levels is deregulated in melanoma cells through BRAF-MEK-ERK signaling. *Oncogene* 24, 3459–3471 (2005).
- W. E. Damsky, D. P. Curley, M. Santhanakrishnan, L. E. Rosenbaum, J. T. Platt,
 B. E. G. Rothberg, M. M. Taketo, D. Dankort, D. L. Rimm, M. McMahon, M. Bosenberg,
 β-Catenin signaling controls metastasis in Braf-activated Pten-deficient melanomas.
 Cancer Cell 20, 741–754 (2011).

SCIENCE SIGNALING | RESEARCH ARTICLE

- S. Spranger, R. Bao, T. F. Gajewski, Melanoma-intrinsic β-catenin signalling prevents antitumour immunity. Nature 523, 231–235 (2015).
- M. Mullooly, P. M. McGowan, S. A. Kennedy, S. F. Madden, J. Crown, N. O' Donovan, M. J. Duffy, ADAM10: A new player in breast cancer progression? *Br. J. Cancer* 113, 945–951 (2015).
- H. Ji, J. Wang, H. Nika, D. Hawke, S. Keezer, Q. Ge, B. Fang, X. Fang, D. Fang,
 D. W. Litchfield, K. Aldape, Z. Lu, EGF-induced ERK activation promotes CK2-mediated disassociation of α-catenin from β-catenin and transactivation of β-catenin. *Mol. Cell* 36, 547–559 (2009).
- B. Bedogni, Notch signaling in melanoma: Interacting pathways and stromal influences that enhance Notch targeting. *Pigment Cell Melanoma Res.* 27, 162–168 (2014).
- T. Golan, A. R. Messer, A. Amitai-Lange, Z. Melamed, R. Ohana, R. E. Bell, O. Kapitansky, G. Lerman, S. Greenberger, M. Khaled, N. Amar, J. Albrengues, C. Gaggioli, P. Gonen, Y. Tabach, D. Sprinzak, R. Shalom-Feuerstein, C. Levy, Interactions of melanoma cells with distal keratinocytes trigger metastasis via notch signaling inhibition of MITF. *Mol. Cell* 59, 664–676 (2015).
- A. H. Shain, I. Yeh, I. Kovalyshyn, A. Sriharan, E. Talevich, A. Gagnon, R. Dummer, J. North, L. Pincus, B. Ruben, W. Rickaby, C. D'Arrigo, A. Robson, B. C. Bastian, The Genetic evolution of melanoma from precursor lesions. *N. Engl. J. Med.* 373, 1926–1936 (2015).
- H.-J. Ma, G. Zhao, S.-X. Zi, D.-G. Li, W. Liu, Q.-Q. Yang, Efficacy of quantifying melanosome transfer with flow cytometry in a human melanocyte–HaCaT keratinocyte co-culture system in vitro. *Exp. Dermatol.* 19, e282–e285 (2010).
- B. S. Lee, S. H. Kim, J. Oh, T. Jin, E. Y. Choi, S. Park, S.-H. Lee, J. H. Chung, S.-M. Kang, C-reactive protein inhibits survivin expression via Akt/mTOR pathway downregulation by PTEN expression in cardiac myocytes. *PLOS ONE* 9, e98113 (2014).

Acknowledgments: We thank R. Zeidler for providing antibodies for melanoma screening. We thank A. Wild, M. Eberhardt, G. Santos-Rosales, and J. Vera-Gonzalez for support for the statistical analyses. Funding: This work was supported by funds from the German Science Foundation (DFG): SFB 643 (J.-H.L.). J.D. was supported by funds from the German Federal Ministry of Education and Research (BMBF) under grant 01GU1107A. S. Schierer is supported by the IZKF (Interdisziplinäre Zentrum für Klinische Forschung) Erlangen. C.O. is supported by the Comprehensive Cancer Center Erlangen. Author contributions: A.S.B. conceptualized and coordinated the project; C.O. performed the antibody screening and MELC analysis; J.-H.L. performed the transfections, protein analysis, and protease activity assays; S. Schierer cloned the adenoviral constructs; K.B., S.W., J.D., and L.C. performed the transfections and confocal analysis using adenoviral constructs; E.K. performed the selection and amplification of antibodies; B.S. and S. Schliep performed and analyzed the immunohistochemistry; G.S. provided expertise and feedback and set up the MELC technology. Competing interests: The authors declare that they have no competing interests.

Submitted 17 August 2016 Accepted 23 February 2017 Published 14 March 2017 10.1126/scisignal.aai8288

Citation: C. Ostalecki, J.-H. Lee, J. Dindorf, L. Collenburg, S. Schierer, B. Simon, S. Schliep, E. Kremmer, G. Schuler, A. S. Baur, Multiepitope tissue analysis reveals SPPL3-mediated ADAM10 activation as a key step in the transformation of melanocytes. *Sci. Signal.* 10, eaai8288 (2017).